

# Surface wave effects on water temperature in the Baltic Sea: simulations with the coupled NEMO-WAM model

Victor Alari<sup>1,2</sup> · Joanna Staneva<sup>1</sup> · Øyvind Breivik<sup>3</sup> · Jean-Raymond Bidlot<sup>4</sup> · Kristian Mogensen<sup>4</sup> · Peter Janssen<sup>4</sup>

Received: 2 November 2015 / Accepted: 1 June 2016  
© Springer-Verlag Berlin Heidelberg 2016

**Abstract** Coupled circulation (NEMO) and wave model (WAM) system was used to study the effects of surface ocean waves on water temperature distribution and heat exchange at regional scale (the Baltic Sea). Four scenarios—including Stokes–Coriolis force, sea-state dependent energy flux (additional turbulent kinetic energy due to breaking waves), sea-state dependent momentum flux and the combination these forcings—were simulated to test the impact of different terms on simulated temperature distribution. The scenario simulations were compared to a control simulation, which included a constant wave-breaking coefficient, but otherwise was without any wave effects. The results indicate a pronounced effect of waves on surface temperature, on the distribution of vertical temperature and on upwelling's. Overall, when all three wave effects were accounted for, did the estimates of temperature improve compared to control simulation. During the summer, the wave-induced water temperature changes were up to 1 °C. In northern parts of the Baltic Sea, a warming of the surface layer occurs in the wave included simulations in summer months. This in turn reduces the cold bias between simulated

and measured data, e.g. the control simulation was too cold compared to measurements. The warming is related to sea-state dependent energy flux. This implies that a spatio-temporally varying wave-breaking coefficient is necessary, because it depends on actual sea state. Wave-induced cooling is mostly observed in near-coastal areas and is the result of intensified upwelling in the scenario, when Stokes–Coriolis forcing is accounted for. Accounting for sea-state dependent momentum flux results in modified heat exchange at the water-air boundary which consequently leads to warming of surface water compared to control simulation.

**Keywords** Wave-ocean coupling · NEMO · WAM · Baltic Sea · Temperature

## 1 Introduction

### 1.1 Theoretical background

The numerical modelling of hydrodynamic processes is separated into two basic disciplines: spectral wave modelling, where the wave energy density spectra (statistical/integrated parameters) is calculated and modelling of the mean flow based on Navier–Stokes equations. One reason for the separation is the different time scales of the processes investigated—while typical wind wave periods range from 1–20 s, the typical time scales of water movement ranges from hours to years. A more important reason is probably the complexity of joining two widely different modelling approaches. Separation between the two basic disciplines is a pragmatic way of studying water bodies which can work well, especially for the wave model which is largely insensitive to the interior ocean except in areas with refraction due to strong currents

---

Responsible Editor: Birgit Andrea Klein

---

✉ Victor Alari  
victor.alari@hzg.de

<sup>1</sup> Helmholtz-Zentrum Geesthacht, Max-Planck Strasse 1, 21502 Geesthacht, Germany

<sup>2</sup> Marine Systems Institute at Tallinn University of Technology, Akadeemia tee 15a, 12611 Tallinn, Estonia

<sup>3</sup> Norwegian Meteorological Institute, Henrik Mohns Plass 1, 0313 Oslo, Norway

<sup>4</sup> European Centre for Medium-Range Weather Forecasts (ECMWF), Shinfield Park, Reading RG29AX, United Kingdom

(Komen et al. 1994), but it violates energy and momentum conservation and will thus affect the upper ocean.

Measurements, as well as theoretical, numerical and laboratory studies, have been conducted to explain the physical mechanisms through which surface waves interact with the flow and ocean processes (like turbulent mixing, Langmuir circulation, etc.) and mediate the momentum flux from air to sea. Longuet-Higgins and Stewart (1962) studied the changes in mean sea level produced by surface waves and indicated the importance if including the radiation stress. Hasselmann (1970) showed that Stokes drift generated by surface waves interacts with the planetary vorticity and suggested that the Stokes-Coriolis force should be taken into account as an additional term in the momentum equations. The instability arising from the non-linear interactions between the Stokes drift profile and the wind-driven currents was shown by Craik and Leibovich (1976) to be a possible explanation for Langmuir circulation. Janssen (1989) proposed that the stress that the water feels depends not only on the wind speed but also on the wave field. Several studies showed that breaking waves (whitecaps) increase turbulence in the upper part of water column (Craig and Banner 1994; Gemmrich and Farmer 2004; Gemmrich 2010). Schneggenburger et al. (2000) use wave-turbulence interaction as a dissipation source function. Babanin (2006) found that non-breaking waves are able to create turbulence, if the wave-amplitude-based Reynolds number exceeds a critical value. Ardhuin and Jenkins (2006) found that as if the Stokes drift shear were a mean flow shear producing turbulence. Qiao et al. (2004) used wave-induced turbulent viscosity and applied it in a global ocean circulation model.

## 1.2 Wave effects on circulation

Several studies found that including these wave effects in a circulation model improves the skill of the simulated data. Dietrich et al. (2011) found an improvement of modelled surge heights in hurricanes in the Gulf of Mexico, when the radiation stress was taken into account. A better agreement between measured and modelled sea surface temperature (SST), when wave-induced breaking was accounted for, is demonstrated by Mellor and Blumberg (2004). Polton et al. (2005) demonstrated that taking the Stokes-Coriolis forcing into account shows encouraging agreement between model and measurements of the mixed layer; significant improvement of modelled surge heights when the wave-dependent drag was taken into account is demonstrated by Mastenbroek et al. (1993) and Bertin et al. (2015); Janssen (2012) showed positive impact of wave breaking on the simulations of daily cycle of sea surface temperature, and just recently, Breivik et al. (2015) demonstrated reduced bias between modelled and measured water temperature by

incorporating the Stokes-Coriolis forcing, turbulence induced by breaking waves and ocean side stress into the NEMO model.

Until now, the impact of wave processes on the circulation and mixing in the Baltic Sea has seldom been studied, compared for example to the North Sea (Pleskachevsky et al. 2009; Pleskachevsky et al. 2011; Grashorn et al. 2015). Axell (2002) studied the impact of Langmuir circulation on vertical distribution of salinity and found that the thickness of the upper mixed layer deepens by 8 m in the southern Baltic Sea. Kantha et al. (2010) studied the Stokes production of turbulent kinetic energy and found that in the mixed layer, it is of the same order of magnitude as the shear production. The importance of the Langmuir turbulence described by the Langmuir number was also pointed out by Belcher et al. (2012). It has also been shown that due to the radiation stress, waves increase the surge height in small bays during extreme storms (Alari and Kõuts 2012) and in shoaling zones; they induce currents similar order of magnitude than wind-driven currents (Raudsepp et al. 2011). Carlsson et al. (2009) studied the impact of swell on atmospheric momentum flux and found that current velocity and surface stress were significantly altered during periods of low wind speed in the presence of swell.

## 1.3 Objectives and method

The aim of this work is to study the influence of wind waves on the water temperature distribution in the Baltic Sea. In this study, we aim to make use and further develop and provide a scientific basis for the operational service implementation in COPERNICUS CMEMS of the achievements on the coupling of circulation and wave models. Therefore, the state of the art circulation model NEMO and the wave model WAM (WAMDI 1988; Komen et al. 1994; ECMWF 2015) are used in order to support the future production of more consistent ocean-marine weather information including on surface waves, which is often requested by users. The coupling between the NEMO and WAM models was investigated by Breivik et al. (2015) to study the effects of coupling on global scales both in the context of an ocean model driven by wave forcings and a fully coupled atmosphere-ocean-wave model. Here, we demonstrate the importance of coupling on regional scales and focus on the Baltic Sea. This is the first three-dimensional ocean circulation study for the whole Baltic Sea, which takes into account several wave effects. The necessity of taking into account wave effects to circulation in a regional sea has been discussed before in the context of a single physical effect (Langmuir circulation—Tuomi et al. 2012a; Radiation stress—Alari and Kõuts (2012)), but the joint and individual contribution of different physical effects has not been addressed before.

The structure of the paper is as follows. In Section 2, we give a brief overview of the general physical features of the Baltic Sea; we describe the coupled model components and its setup. We also list the data used for validation. In Section 3, we describe the wave processes included in the circulation model. In Section 4, we will describe the wave model performance. In Section 5, we describe the impact of waves to water temperature. The main findings are summarized in Section 6.

## 2 Study area, methods and data

### 2.1 Study area

The Baltic Sea is a large seasonally ice-covered water body which spans from 9 to 30° E and 53 to 66° N. Its total area is 435,000 km<sup>2</sup>. The basin contains several topographically and geographically defined sub-basins (Fig. 1a). The mean water depth is 55 m, and the maximum water depth reaches 459 m in the Landsort Deep. Limited water exchange with the North Sea (through the Danish straits) and considerable freshwater input from the rivers lead to a mean salinity of about 7 g/kg. The combined input of salty and fresh water permits permanent stratification, where the halocline is located between 60 and 80 m (Väli et al. 2013). The seasonal thermocline starts to build in April, is located at about 20 m in summer and erodes down to 60 m in December (Leppäranta and Myrberg 2009). Cold intermediate layer is also observed in the deeper areas of the Baltic Sea, between the depths of 30–60 m (Leppäranta and Myrberg 2009).

Due to the geometry of the Baltic Sea and its geographical location, the surface wave field exhibits large spatial and temporal variations. Monthly mean and monthly maximum wave heights in autumn-winter are twice as high compared to spring-summer months (Tuomi et al. 2011), and the Baltic Proper (BP; see Fig. 1 for location) has the highest waves. Instrumentally measured maximum significant wave height was 8.2 m in the northern Baltic Proper, 7.4 m in the southern Baltic Proper and 5.2 m in the Gulf of Finland (Tuomi et al. 2011). Modelled significant wave height can reach up to 10 m (Soomere et al. 2008; Tuomi et al. 2011), and 100-year return estimates based on the NORA10 archive suggest (Reistad et al. 2011) wave heights up to 12 m (Aarnes et al. 2012).

### 2.2 Model description and setup

NEMO (Nucleus for European Modelling of the Ocean) is a framework of ocean-related engines, from which we use the OPA package (for the ocean dynamics and thermodynamics) and the LIM2 sea-ice dynamics and thermodynamics package (Madec 2008; Bouillon et al. 2009). In OPA, six primitive equations (momentum balance, the hydrostatic equilibrium, the incompressibility equation, the heat and salt conservation

equations and an equation of state) are solved, where Arakawa C grid is used in horizontal. For detailed description of the model equations, see Madec (2008). In the vertical terrain-following coordinates, *z*-coordinates or hybrid *z-s* coordinates can be used. For a complete description of the model, see Madec (2008). Previously, NEMO has been applied for the Baltic Sea area in uncoupled mode (Hordoir et al. 2013) and coupled to atmospheric models (Dieterich et al. 2013; Pham et al. 2014).

The wave model WAM (The WAMDI group 1988; ECMWF 2015) is a third-generation wave model, which solves the action balance equation without any a priori restriction to the evolution of spectrum. It has been extensively used for modelling the Baltic Sea wave fields (Soomere 2003; Soomere 2005; Soomere et al. 2008; Tuomi et al. 2011; Tuomi et al. 2012b; Tuomi et al. 2014). The action density spectrum *N* is considered instead of the energy density spectrum *E* because in the presence of ambient currents, action density is conserved, but energy density is not. Action density is related to energy density through the relative frequency (Whitham 1974):

$$N(\sigma, \theta) = \frac{E(\sigma, \theta)}{\sigma} \tag{1}$$

The variable  $\sigma$  is the relative frequency (as observed in a frame of reference moving with the current velocity) and  $\theta$  is the wave direction (the direction normal to the wave crest of each spectral component). The action balance equation in Cartesian coordinates reads:

$$\begin{aligned} \frac{\partial N}{\partial t} + (\mathbf{c}_g + \mathbf{U}) \nabla_{x,y} N + \frac{\partial c_\sigma N}{\partial \sigma} + \frac{\partial c_\theta N}{\partial \theta} \\ = \frac{S_{wind} + S_{nl4} + S_{wc} + S_{bot}}{\sigma} \end{aligned} \tag{2}$$

On the left-hand side of Eq. (2), the first term represents the local rate of change of action density in time; the second one denotes the propagation of wave energy in two dimensional geographical space, where  $\mathbf{c}_g$  is the group velocity vector and  $\mathbf{U}$  the ambient current vector. The third term represents shifting of the relative frequency due to variations in depths and currents (with propagation velocity  $c_\sigma$  in  $\sigma$  space). The fourth term represents depth-induced and current-induced refraction (with propagation velocity  $c_\theta$  in  $\theta$  space). At the right-hand side of the action balance equation is the source term that represents physical processes which generate, redistribute, or dissipate wave energy in the WAM model. These terms denote, respectively, energy input by the wind  $S_{wind}$ , non-linear transfer of wave energy through four-wave interactions  $S_{nl4}$  and wave dissipation due to whitecapping  $S_{wc}$  and bottom friction  $S_{bot}$ .

Both models share the same computational grid and bathymetry with horizontal resolution of 2 nautical miles

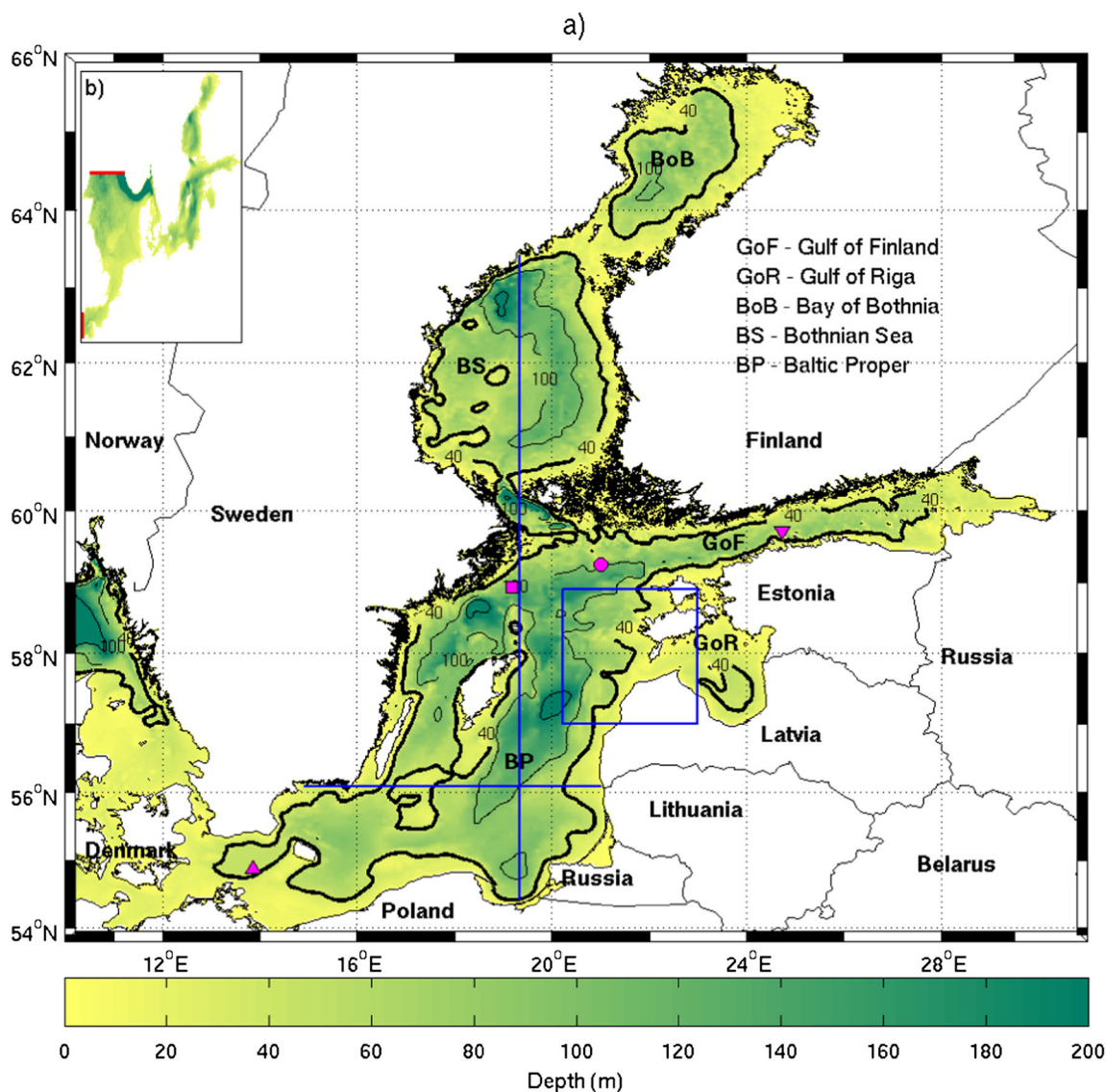


**Fig. 1** Topography of study area with buoy station locations and transects (blue lines), where vertical profile of temperature is analysed. Area bounded by blue box is where model is compared to MODIS data.

The buoy stations read: Arkona (*triangle*), Huvudskarost (*square*), NBP (*circle*) and Tallinna madal (*inverted triangle*)

covering the Baltic Sea and the North Sea (Fig. 1). In the vertical, NEMO was set up with  $z$ -coordinates at 56 levels. The spectrum in WAM was discretized with 24 directions and 25 frequencies. The hourly atmospheric forcing is based on the German Weather Service (DWD) short range forecasts (24 h), and we use bulk formulation in NEMO. The open boundaries of the model domains are located in west of English Channel and near the continental shelf break of the North Sea (Fig. 1b). At the open boundaries, tidal amplitudes and velocities are prescribed as well as climatological temperature and salinity. The wave model starts from rest (cold-start), while the ocean model uses Janssen et al. (1999) climatology. The analysed period is the year from October 2012 until September 2013. This period is long enough for the simulation of important features of the Baltic Sea, e.g. the formation

of cold intermediate layer, evolution of thermocline and upwellings. The first 7 months are used as a spin-up, and during that period, LIM2 ice model is also activated. Details of model setup can be found in Table 1.

### 2.3 Measured data

In this paper, we use in situ data and remote sensing data in order to assess the quality of the different simulations of the model system. For the evaluation of basin scale sea surface temperature, we compare model simulations with the OSTIA (Operational Sea Surface Temperature and Sea Ice analysis) dataset. OSTIA uses satellite data together with in situ observations to determine the sea surface temperature. The analysis is performed using a variant of optimal interpolation. The

**Table 1** Details of model simulation

Parameter/ model	NEMO (version 3.4)	WAM (version CY40R3)
Modelling period	01.10.2012–30.09.2013	Switched on at 01.05.2013
Horizontal grid	2 nautical miles covering North Sea and Baltic Sea	Same horizontal grid. Spectral resolution: 24 directions and 25 frequencies
Vertical grid	56 z layers	N/A
Integration timestep(s)	10 s for barotropic part; 180 s for baroclinic part	30 s
Initial field	Janssen et al. (1999) climatology for T & S	Coldstart
Boundary condition	OSU tides, Janssen et al. (1999) climatological periodic boundary	No
Atmospheric forcing	German Weather Service (DWD), 1 h. Meridional and zonal wind speed; shortwave and longwave radiation; air temperature; humidity; air pressure	Same source, but only wind components
Vertical diffusion scheme	Generic length scale ( $k-\epsilon$ ), Umlauf and Burchard (2003)	N/A
Ice	LIM2	No ice, as wave model input was used starting from May

analysis is produced daily at a resolution of ca 5 km (for further details, see Donlon et al. 2011). The OSTIA data was interpolated to NEMO computational grid, and the bias of sea surface temperature between model and OSTIA was calculated for the Baltic Proper region.

From the MyOcean database (<http://www.myocean.eu>), we extracted vertical profile measurements taken at the location 58.93° N, 19.17° E (see Fig. 1). This station is a representative for the Baltic Proper area and for other Gulfs as well, where the water is deep enough to allow for the cold intermediate layer to develop. The measurements were taken at levels 5 to 60 m below surface with a 5 m step and then onwards till 90 m with 10 m step. However, some of the deeper layer data are absent. Modelled sea surface temperature was also compared with two other stations, one in the southern Baltic Sea and one in the Gulf of Finland (see Fig. 1a for specific locations). Significant wave height was validated with measurements taken by Finnish Meteorological station at a location 58.25° N, 21° E at northern Baltic Proper. Finally, SST as observed by MODIS (Moderate Resolution Imaging Spectroradiometer; standard level 2 MODIS SST product available at <http://oceancolor.gsfc.nasa.gov>) was used to compare the extent and structure of an

upwelling. The image was acquired for 24.07.2013 10:25 UTC with a 1 × 1-km pixel spacing.

### 3 Wave effects in the ocean model

Ocean waves influence the circulation through number of processes: turbulence due to breaking and non-breaking waves, momentum transfer from breaking waves to currents in deep and shallow water, wave interaction with planetary and local vorticity, Langmuir turbulence. The NEMO ocean model has been modified to take into account the following wave effects: (1) The Stokes-Coriolis forcing (Hasselmann 1970); (2) Sea-state dependent momentum flux (Janssen 1989; Janssen 2012); and (3) Sea-state dependent energy flux (Craig and Banner 1994). Here, we describe in detail the wave-circulation interaction mechanisms that have been implemented in NEMO. The applicability of the used approach for the global ocean has been previously addressed in Breivik et al. (2014) and Breivik et al. (2015). A schematic overview of these processes is shown on Fig. 2. Below, we will give a brief description of each of them. For a more detailed description, the reader is referred to Breivik et al. (2015).

#### 3.1 Stokes-Coriolis forcing

Fluid particle trajectories in water waves are not perfectly circular (in deep water) or elliptical (in intermediate water) due to several reasons. First is the loss of the orbital motion due to turbulence of all kind (not accounted in this study). Second is, in practice, in the presence of the wave spectrum; the combination of different wave components result in a non-closed particle trajectory, due to particle drift by second and third main wave components. This different speed of wave crests and troughs sets up a difference between the average Lagrangian flow velocity of a fluid parcel and the Eulerian flow velocity, the Stokes drift (Stokes 1847). Though the mean Stokes drift speed is small, even in a moderate storm, where the significant wave height reaches 3.5 m (Fig. 3a, 22 July 2013), the Stokes drift (Fig. 3b) can reach up to 0.35 m/s and in extreme conditions up to 1.35 m/s at the surface of the Baltic Sea (not shown here). This implies that Stokes drift speed in extreme weather conditions is of the same order of magnitude as wind forced currents at surface, as the surface Ekman current speed is approximately 2 % of the wind speed (Chang et al. 2012).

In this study, we assumed irrotational fluid. However, in reality, the fluid is viscous. Albeit small and negligible from the point of view of many applications, water viscosity is not zero. Such turbulence arising from the fact that water is viscous is not accounted in this study but has been taken into account before, e.g. Schneggenburger et al. 2000.

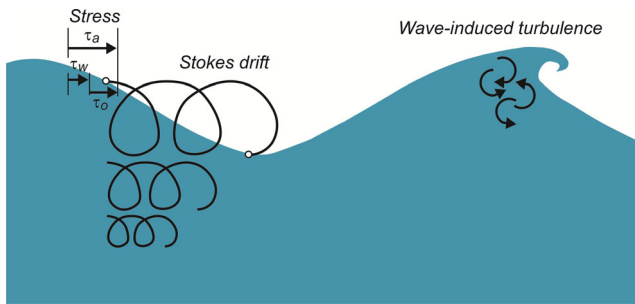


**Fig. 2** Wave-ocean interaction mechanism's included in this study

Like wind-induced currents, the Stokes drift is also influenced by the Earth's rotation and it adds an additional veering to the ocean currents known as the Stokes-Coriolis force:

$$\frac{D\mathbf{u}}{Dt} = -\frac{1}{\rho}\nabla p + (\mathbf{u} + \mathbf{v}_S) \times f\hat{\mathbf{z}} + \frac{1}{\rho}\frac{\partial\tau}{\partial z} \quad (3)$$

where  $\mathbf{v}_S$  is the Stokes drift vector,  $p$  is the pressure,  $\tau$  is the surface stress and  $\hat{\mathbf{z}}$  is the upward unit vector. Because calculating the full vertical profile is costly, the Stokes drift velocity profile is calculated with an approximation given by Breivik et al. (2014).

### 3.2 Sea-state dependent momentum flux

As waves grow, they absorb momentum from the atmosphere. The ocean current therefore feels less stress. In this case, the ocean side stress  $\tau_{oc}$  is the atmospheric stress  $\tau_a$  minus the momentum flux absorbed by waves  $\tau_{in}$ :

$$\tau_{oc} = \tau_a - \tau_{in} \quad (4)$$

Waves release momentum to the ocean when they break and therefore the ocean side stress becomes

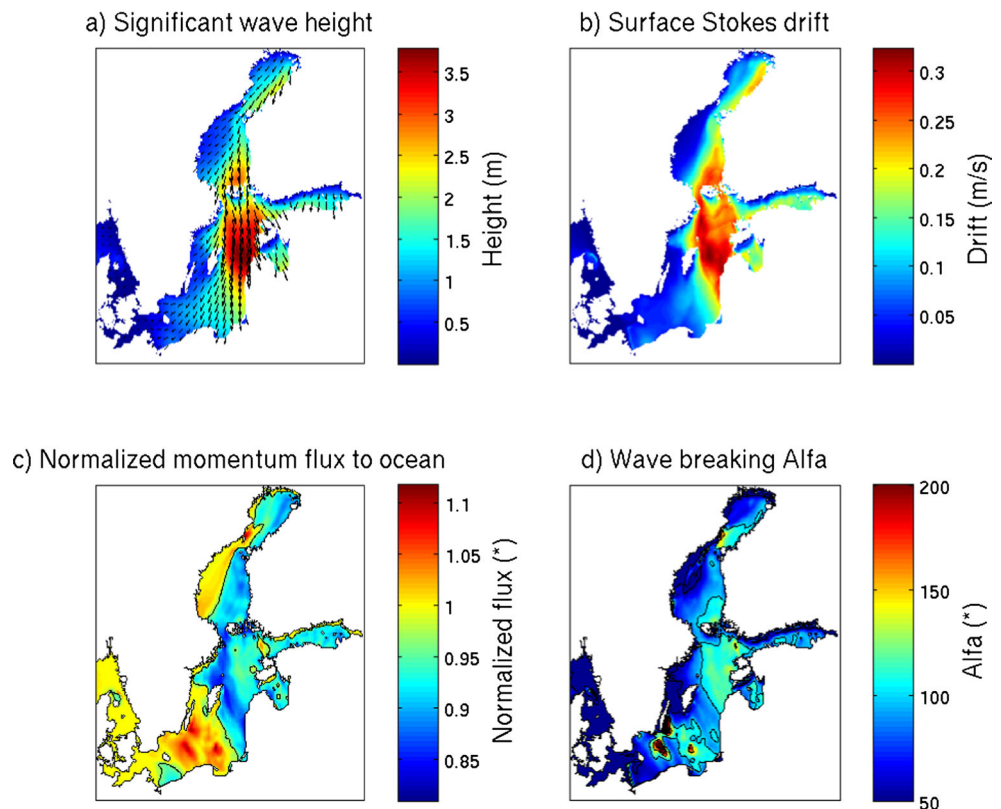
$$\tau_{oc} = \tau_a - \tau_{in} - \tau_{db} \quad (5)$$

where  $\tau_{db}$  is the momentum injected by breaking waves (negative). Only if the input of momentum by wind is balanced by the release of momentum through breaking (fully developed sea) will the ocean side stress balance the atmospheric stress. Most of the time waves are not fully developed and the ocean side stress differs from the atmospheric stress by 5–10% and in extreme cases by 20–30%. Therefore, sea-state dependent surface stress is considered instead of bulk formulae.

The normalized momentum flux

$$\tilde{\tau} = \frac{\tau_{oc}}{\tau_a} \quad (6)$$

**Fig. 3** Wave processes during a northerly storm on 22 July 2013 at 19:00 UTC. On **a**, every 10th wave direction vector is shown



is shown on Fig 3c. In the region of active wave growth, the normalized momentum flux is below 1 (see black contour line on Fig. 3c), meaning that the ocean side stress is less than the atmospheric stress. In areas where waves have travelled outside the area of wind which can sustain the waves, the waves are decreasing and releasing momentum to the ocean through wave breaking. There, the normalized momentum flux is above 1.

### 3.3 Sea-state dependent energy flux

In NEMO, wave-induced turbulent kinetic energy (TKE) depends on the wave energy factor  $\alpha$  (Craig and Banner 1994). It is set to a constant value regardless of sea state, because Craig and Banner (1994) argued that the turbulent kinetic energy flux is well approximated by  $\alpha u_*^3$  where the value of  $\alpha = 100$  is a reasonable average, but concede that values should lie in the range 50 to 150 for young to mature seas. It has been argued by Gemmrich et al. (1994) that a better approach would be to use an effective wave propagation speed, but we choose instead to compute the TKE flux directly from the integrated source terms of the wave model, thus giving us the exact energy input from the wave model. With access to a full spectral wave model, it is possible to estimate the momentum flux from breaking waves and therefore to calculate  $\alpha$ . In Fig. 3d, we show the spatial distribution of  $\alpha$  on 22 July 2013. While in many areas it is near 100 (see the black contour line), it actually varies between 10 and up to 500, depending on the dissipation intensity (and since it is normalised by the cube of the friction velocity, it is also sensitive to sudden changes in wind speed). We use  $\alpha$  estimated by WAM when waves are accounted for in our NEMO simulations and use the standard value of 100 in our control experiment.

We note that wave breaking during a storm can introduce strong turbulence in the water column, but this source of turbulence is limited to the upper water layer and this propagation into the depth may have too long spin-up time, to reach the depths of 30–50 m during a storm peak. After the storm peak has passed, the waves are no longer as high and steep for breaking, and therefore, the whitecapping is too minor a turbulence source to influence the whole water column. Therefore, in future studies, the turbulence due to non-breaking waves should also be considered.

In NEMO, the boundary condition of the turbulent length scale  $z_0$  on the water side of the air-sea interface follows the Charnock relation:

$$z_0 = \frac{\beta u_{w*}^2}{g} \quad (7)$$

where  $u_{w*}$  is the water-side friction velocity,  $\beta$  is the Charnock constant and  $g$  is the acceleration due to gravity.

The turbulent length scale in water is orders of magnitudes larger compared to its analogue in air side.

In the default version of NEMO, the Charnock constant has a value of  $2 \cdot 10^5$ , which was the value found by Stacey (1999) by minimizing the errors between measured and modelled currents. Moreover, Stacey (1999) found that  $z_0$  is in the order of significant wave height, while others have found it to be in the order of wave amplitude up to significant wave height (Craig and Banner 1994; Terray et al. 1996; Drennan et al. 1996). In this study, we also make the assumption that  $z_0$  scales with significant wave height, based on the findings of previous work (Craig and Banner 1994; Terray et al. 1996; Drennan et al. 1996), and therefore, in NEMO, we substitute  $z_0$  with significant wave heights (in the wave included runs) when latter is greater than 0, and keep  $\beta$  constant (1400) when significant wave height is 0. In that sense, Fig. 3a represents also the turbulent length scale on the water side of the air-sea interface if waves are present.

### 3.4 Test cases

For the control simulation (experiment CTRL), NEMO is run without a wave model but the energy flux from breaking waves is parameterized according to Craig and Banner (1994) and Mellor and Blumberg (2004) with  $\alpha = 100$  and the water-side Charnock constant  $\beta = 1400$ . This control simulation is compared with simulations which include the wave effects described in Section 3.1–3.3. In these simulations, either all three wave effects (experiment ALLWAVE) are activated or the individual mechanisms are taken into account separately to determine the effect of each process. The three additional simulations in which the individual processes considered are sea-state dependent momentum flux (experiment TAUOC), sea-state dependent energy flux (experiment BREAK) and Stokes-Coriolis forcing (experiment STCOR). The experiments are summarized in Table 2.

## 4 Validation of simulated waves and temperature

In this section, we will describe the wave model performance by comparing significant wave height simulated with WAM to the wave measurements taken at northern Baltic Proper. Simulated sea surface temperature (SST) and vertical profiles of temperature are compared to several measurements in order to assess the performance of the model simulations.

The WAM simulated significant wave height compares very well with the one from the measurements (Fig. 4) during June, July and August (JJA) 2013, with a correlation coefficient of 0.97. Though the model tends to overestimate high wave events in the first half of the summer, the overall bias (mean of simulated data minus mean of measured data) is 7 cm. As the waves mostly reflect the quality of the forcing

**Table 2** Summary of model experiments

Simulation	Description of simulations
CTRL	Control simulation, without wave model
ALLWAVE	All three wave processes included
TAUOC	Sea-state dependent momentum flux included only
BREAK	Sea-state dependent energy flux included only
STCOR	Stokes-Coriolis forcing included only

winds, we can conclude that the DWD 1 hourly wind input is adequate to describe the conditions over the Baltic Proper area.

The SST simulated with NEMO model as compared to OSTIA shows a time-varying bias in the Baltic Proper (Fig. 5), with the NEMO being colder than OSTIA data. In general, the bias is more evident at the beginning of summer, while at the end of summer, it stabilizes around  $-1\text{ }^{\circ}\text{C}$ . Such a bias is quite acceptable considering that the simulation does not include any data assimilation. However, by taking into account the three wave effects, the SST bias is reduced by

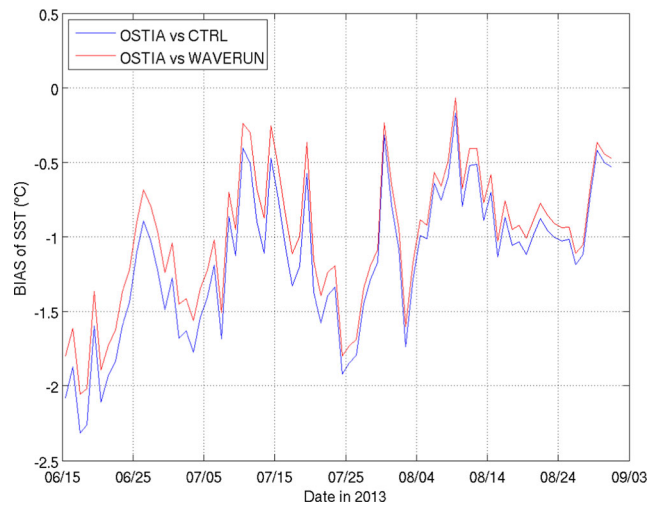


**Fig. 5** Bias (model mean minus mean of measurements) of simulated SST with respect to OSTIA data. The comparison is for an area which roughly corresponds to the borders of the Baltic Proper (see Fig. 1)

$\sim 0.2\text{ }^{\circ}\text{C}$ . We also compared SST from point measurements in three stations scattered over the Baltic Sea and found that

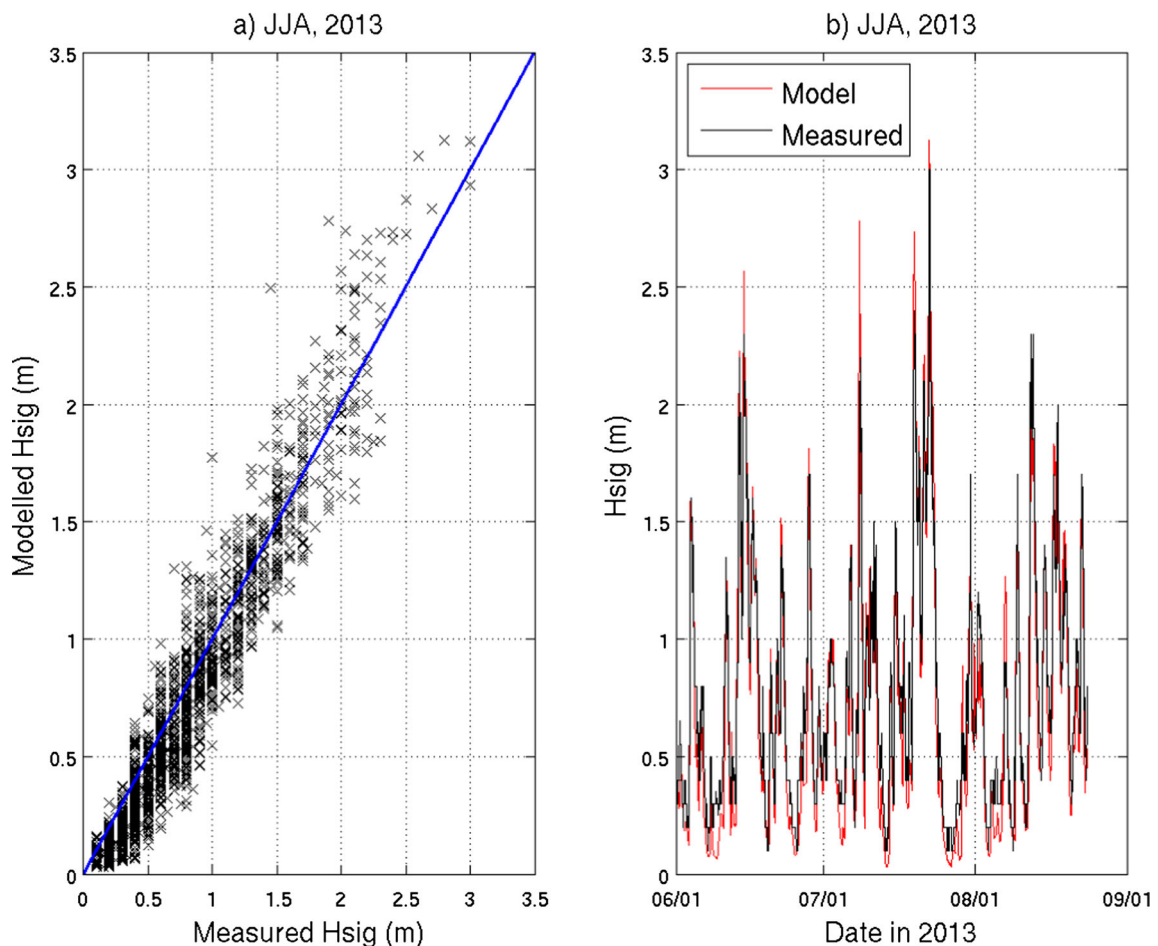


**Fig. 4** Significant wave height ( $H_s$ ) validation at a buoy station located in the Northern Baltic Proper (see Fig. 1). Scatter plot (a) and time-series (b) comparison is presented. The 1:1 line of measurements and model is shown with blue colour



**Table 3** Statistics (01.06.2013–31.08.2013) of model-data comparison of SST in three stations: *Tallinn* measured at Tallinna Madal lighthouse in the Gulf of Finland; *Arkona* measured in Arkona basin in the southern Baltic Proper; *Huvud.* Huvudskarost, measured in the northern Baltic Proper. The statistical parameters are the following: *W\_RMSE* root mean square difference of measured data and wave included simulation; *C\_RMSE* root mean square difference of measured data and control

Station	N	W_RMSE (°C)	C_RMSE (°C)	W_BIAS (°C)	C_BIAS (°C)	W_CORR	C_CORR
Tallinn	181	2.28	2.53	-2.13	-2.38	0.97	0.96
Arkona	179	1.51	1.75	-1.26	-1.51	0.95	0.95
Huvud.	184	1.83	2.11	-1.69	-2.01	0.97	0.97

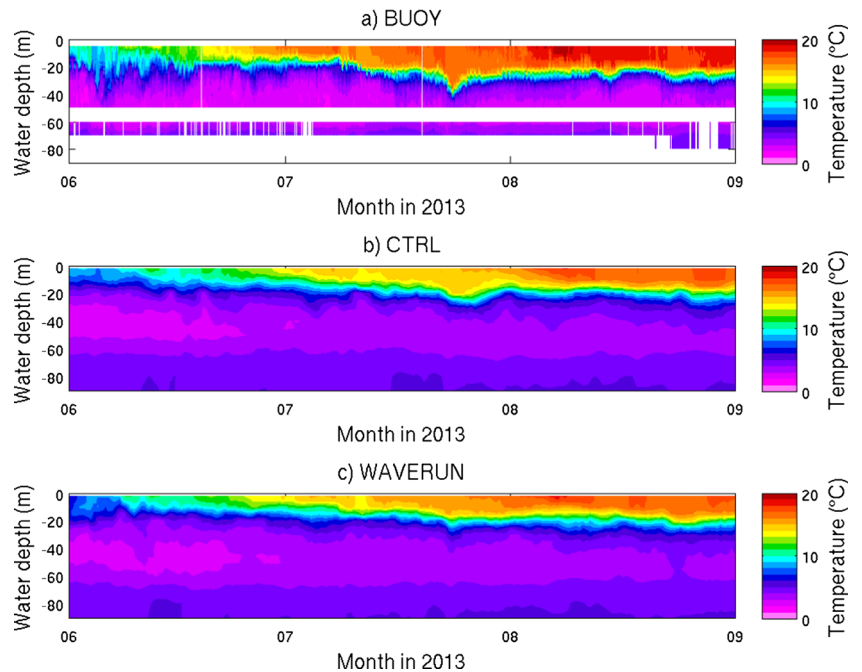
simulation; *W\_BIAS* average difference between wave included simulation and measured data; *C\_BIAS* average difference between control simulation and measured data; *W\_CORR* correlation coefficient between wave included simulation and measured data; *C\_CORR* correlation coefficient between control simulation and measured data. *N* is the number of comparison points

in every case including wave effects improved the quality of the simulated data (Table 3). The cold bias was reduced by up to 0.32 °C and the root mean square difference decreased by up to 0.28 °C.

Comparison of simulated temperature with measurements (Fig. 6) shows that both the control run and the runs with wave effects describe very well the vertical evolution of temperature. The important features, like the seasonal thermocline and the cold intermediate layer, are present in both simulations. The time-evolution of thermocline is also well captured by both simulations, and even the sudden deepening at the end of July is somewhat noticeable. Compared to CTRL, the ALLWAVE run generally yields better results for SST (as was seen in Table 2) and sudden down-bursts of temperature at the beginning of summer. At the end of summer, the wave included simulation also improves the thermocline depth.

Finally, we compare CTRL and ALLWAVE to a MODIS image (Fig. 7a) from a situation where northerly winds caused upwelling of cold water along the eastern coast of the Baltic Proper. The ALLWAVE experiment reduced the bias compared to CTRL experiment by 0.34 °C. It is noteworthy that the structure of upwelling filaments in the ALLWAVE experiment more closely resembles the measurements than does the CTRL experiment. In the ALLWAVE experiment (Fig. 7c), the main upwelling area near Saaremaa Island has the same extension towards the south as in the MODIS, while in the CTRL experiment (Fig. 7b), the upwelling area is fragmented. The intrusion of warm water into the centre of upwelling area near Saaremaa is also more evident in the ALLWAVE experiment, compared to CTRL experiment. Two other upwelling areas, north and south from the one near Saaremaa, are also better captured by the ALLWAVE experiment.

**Fig. 6** Time-depth profiles of measured temperature, control run (CTRL) and the all-wave processes (ALLWAVE) run at station Huvudskarost



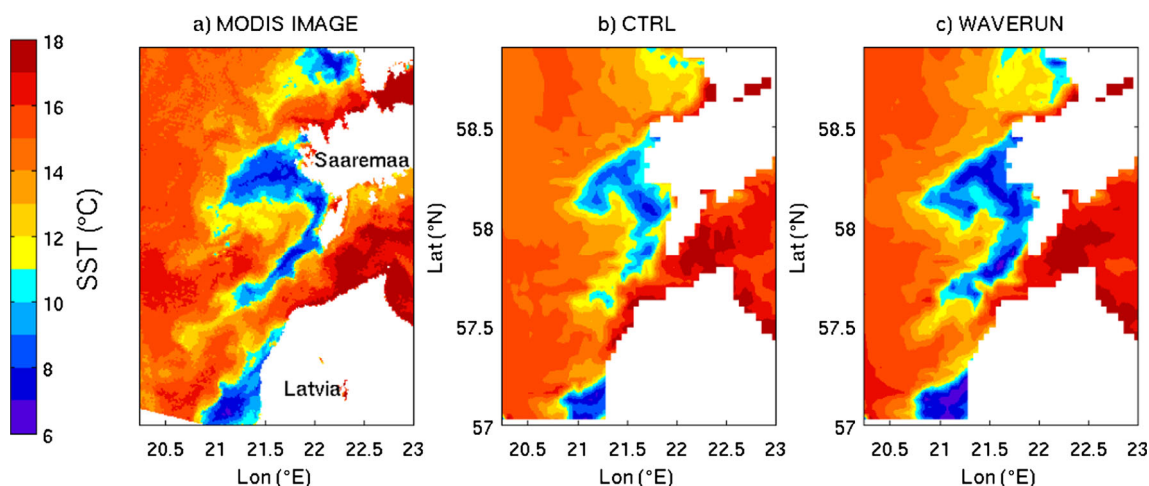


**Fig. 7** Comparison of MODIS SST (*left*), CTRL (*middle*) and ALLWAVE (*right*). The comparison is for 24 July 2013, 12:00 UTC

## 5 Impact of waves

The importance of accounting for wave effects when modelling water temperature has been addressed in the previous sections by comparing with in situ and satellite data. However, the full 3-D impact of waves has to be studied also and this is done in this paragraph for SST, for bottom temperature and for different cross-sections.

### 5.1 Impact of waves on SST and bottom temperature

In this section, we compare the sea surface and bottom temperature between the four scenarios in which the wave effects, described in Section 3, have been taken into consideration (ALLWAVE, STCOR, TAUOC, BREAK, respectively) and the control simulation (CTRL). The aim is to distinguish which of the three mechanisms are dominant in changes of temperature for the different Baltic Sea areas. We calculate the summer averaged (JJA) temperature difference between the four coupled wave-circulation model runs and the control experiment (only NEMO run).

When all the three wave processes are taken into account (Fig. 8a), in every Baltic Sea sub-basin, wave impact on the SST is noticeable. The largest warmings of SST are concentrated to Bay of Bothnia and Bothnian Sea, while the cooling effect of waves becomes most evident near the coasts of eastern Baltic Proper. In order to better understand the processes responsible behind this pattern, we also plot the differences when each wave process is taken into consideration independently (Fig. 8b–d). But note that Fig. 8a is not a linear combination of each wave processes and care should be taken while interpreting them.

In the simulations, wave breaking has mostly a warming effect (Fig. 8b), especially in northern areas of the Baltic Sea. This is because the CTRL experiment has too vigorous mixing

with a wave-breaking coefficient of 100 (see the discussion by Breivik et al. 2015). The impact of Stokes-Coriolis forcing (Fig. 8c) is mostly confined along coastlines and has a cooling effect there. This suggests that Stokes-Coriolis forcing mainly contributes during cases when the conditions are favourable for upwelling. For example, in the northerly storm presented on Fig 3, Stokes drift is pointed towards south, thus strengthening the upwelling. The most ‘large scale’ differences are induced by taking into account wave-dependent momentum flux (Fig. 8d), and the effect is mostly in warming the surface water. By taking into account wave-dependent momentum flux, we indirectly modify the heat exchange at the ocean-air boundary, since turbulent fluxes depend on the stress which is felt by ocean. Directly, the wave-dependent momentum flux affects the currents and therefore the advection of water, which can result in redistribution of cooler/warmer water.

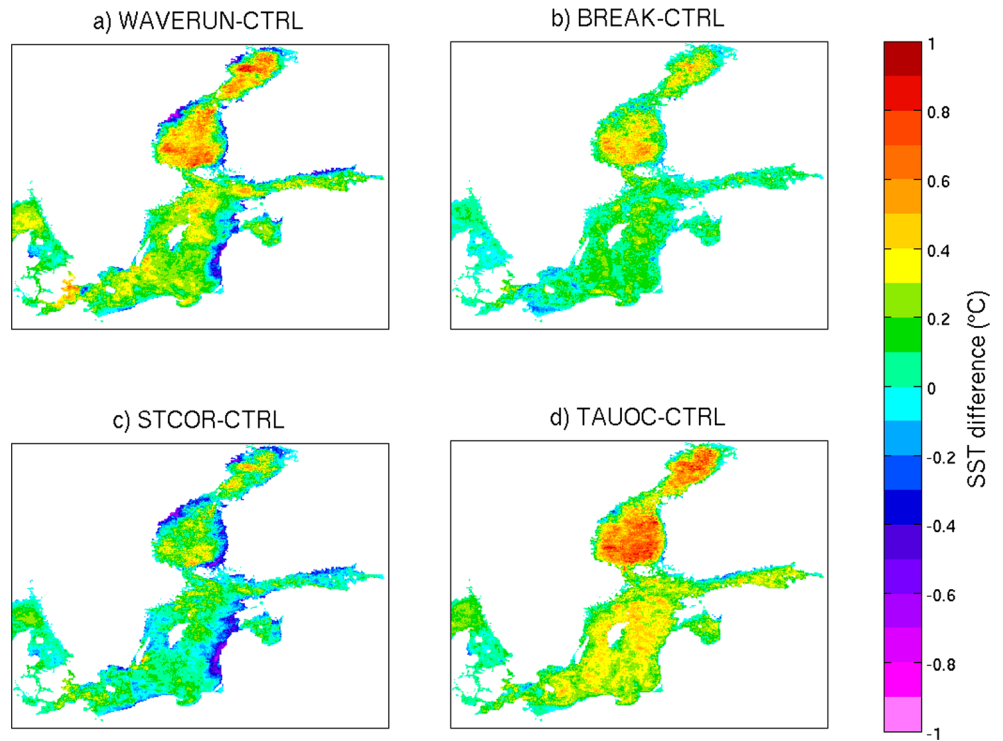
The temperature differences between simulations with wave effects and the control simulation show a general pattern of cooling near the bottom (Fig. 9), especially along the coast although there are some isolated locations where the water temperature increases when wave effects are included. Like in the SST case, most of the coastal cooling is due to Stokes-Coriolis forcing (Fig. 9c); however, here, it seems that all processes also contribute to cooling.

### 5.2 Impact of waves on vertical profiles

We analyse the difference of temperature along a meridional section which maximizes the north–south distance (Fig. 10) and along a zonal section which maximizes west–east distance and covers as much deep water as possible (Fig. 11).

One of the main findings is that wave-induced temperature changes are intermittent along the selected transect lines and along depth levels and at certain locations; the maximum wave effects do not necessarily occur at the surface. The most

**Fig. 8** Sea surface temperature differences between ALLWAVE and CTRL averaged over a 3-month period, from 1 June 2013 to 31 August 2013. The colour bar holds for all panels a to d



prominent differences are found in the upper 30 m. The vertical extent of different wave processes also varies considerably. The TAUOC scenario displays a typical dipole pattern relative to CTRL (Fig. 10c and Fig. 11c) with warmer water at and near the surface and cooler at depths of 20–30 m. The BREAK

scenario shows similar behaviour in the Bothnian Sea (Fig. 10b), but in other sections, the impact of wave breaking is seen only nearer the surface. The STCOR scenario (Fig. 10c and Fig. 11c) shows significant warming below the surface in offshore regions and cooling near the coast.

**Fig. 9** Same as Fig. 8 but for the sea bottom

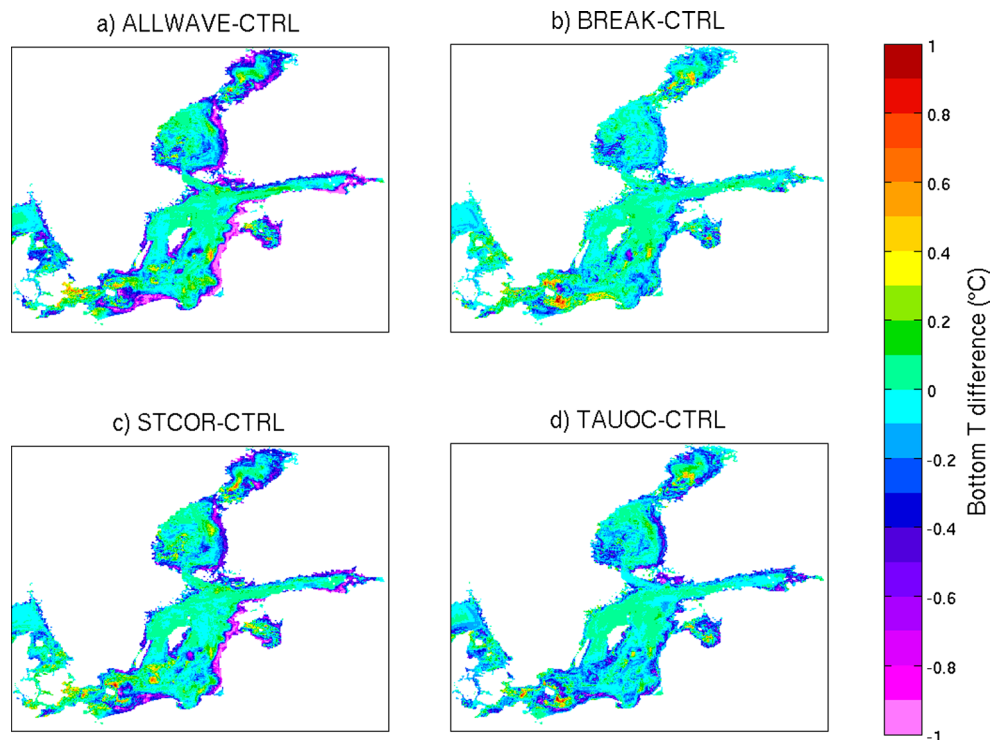
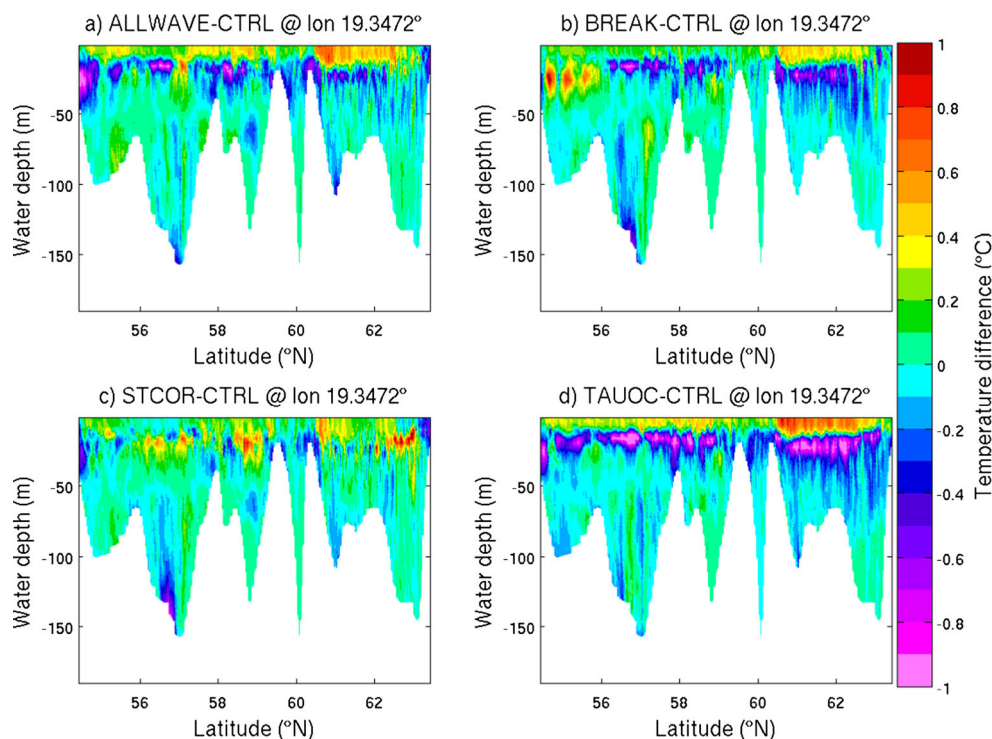


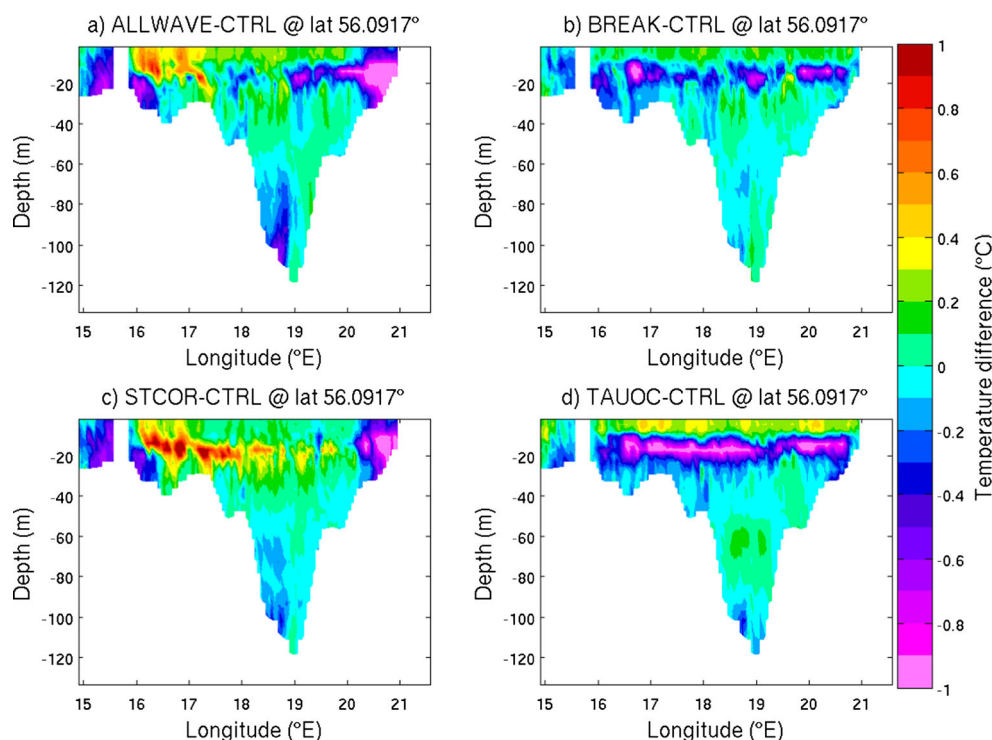
**Fig. 10** Meridional transect of water temperature differences between ALLWAVE and CTRL averaged over a 3-month period, from 1 June 2013 to 31 August 2013. The *colour bar* holds for all panels



Although the validation showed that coupling between a wave model and the ocean model reduces the SST bias, there always remains the question of how realistic the simulation results are as a whole. Specifically—are the changes in water temperature induced by waves in the same range as compared

to other similar studies? Not many full baroclinic model studies have been conducted where the impact of surface waves on temperature has been investigated and there are no studies of this kind at all for the Baltic Sea area. However, a comparison with the existing baroclinic studies (Qiao et al. 2004; Lin et al.

**Fig. 11** Same as Fig. 10 but a zonal transect



2006; Babanin et al. 2009; Warner et al. 2010; Hu and Wang 2010; Qiao et al. 2010; Song et al. 2012; Bai et al. 2013; Zambon et al. 2014; Breivik et al. 2015) suggests that the differences in water temperature between the CTRL simulation and ALLWAVE scenario presented here are realistic.

## 6 Summary and conclusions

The role of the wave-current interaction in the Baltic Sea is just starting to get more attention. In this paper, we took the first step of implementing the coupled NEMO-WAM model on seasonal time scales in a marginal sea area. The main aim was to study the effect of different wave processes on water temperature. Besides, in order to assess the truthfulness of the additional physical processes, we compared the scenario simulations with measurements. In this way, we demonstrated that the performance of the coupled model reproduces spatio-temporal variability of water temperature more truthfully compared to a control simulation. The first results indicate a pronounced effect of waves on the vertical temperature distribution and on meso-scale events. During the summer season, the wave-induced changes were up to 1 °C. The most prominent seasonal warming is located in northern parts of the Baltic Sea in the surface layer. In the bottom layers, cooling usually dominates. Most of the cooling is found in coastal areas and warming in offshore regions. The near-coastal cooling is almost always related to Stokes-Coriolis forcing. This is especially true for deep layers. Compared to other processes, the vertical extent of influence of Stokes-Coriolis forcing is highest. It has the effect of intensifying upwelling near all coasts, depending on the direction of wind. The effect of wave breaking is to warm the surface layer, which in turn reduces the cold bias when comparing model and measured data. This is because the CTRL experiment has too vigorous mixing with a wave-breaking coefficient of 100. The effect of using a wave-modified stress is mostly to warm the surface layer though directly affecting the advection and indirectly the turbulent fluxes.

**Acknowledgments** This work was financially supported through the WAVE2NEMO grant (COPERNICUS). Ø. Breivik acknowledges the MyWave FP7 project (grant FP-7-SPACE-2011-284455). We are grateful for Mrs. Laura Siitam for providing the MODIS image, for Dr. Sebastian Grayek for helping in setting up the NEMO model and for Mrs. Gardeike for helping with the illustration. We also thank the anonymous reviewer for his/her constructive criticism. We thank Finnish Meteorological Institute for providing the measured wave data, Swedish Meteorological and Hydrological Institute for providing in situ temperature profile data and Marine Systems Institute at Tallinn University of Technology for providing SST data.

## References

- Aarnes OJ, Breivik O, Reistad M (2012) Wave extremes in the north-east Atlantic. *J Clim* 25:1529–1543
- Alari V, Kōuts, T (2012) Simulating wave-surge interaction in a non-tidal bay during cyclone Gudrun in January 2005. In *Ocean: Past, Present and Future - 2012 IEEE/OES Baltic International Symposium, BALTIC 2012*, art. no. 6249185
- Ardhuin F, Jenkins AD (2006) On the interaction of surface waves and upper ocean turbulence. *J Phys Oceanogr* 36(3):551–557
- Axell L (2002) Wind-driven internal waves and Langmuir circulations in a numerical ocean model of the southern Baltic Sea. *J Geophys Res*. doi:10.1029/2001JC000922
- Babanin AV, Ganopolski A, Phillips WRC (2009) Wave-induced upper-ocean mixing in a climate model of intermediate complexity. *Ocean Model* 29(3):189–197
- Babanin AV (2006) On a wave induced turbulence and a wave-mixed upper ocean layer. *Geophys Res Lett* 33:L20605
- Bai X, Wang J, Schwab DJ, Yang Y, Luo L, Leshkevich GA, Liu S (2013) Modeling 1993–2008 climatology of seasonal general circulation and thermal structure in the Great Lakes using FVCOM. *Ocean Model* 65:40–63
- Belcher SE, Grant AL, Hanley KE, Fox-Kemper B, Van Roekel L, Sullivan PP, Large WG, Brown A, Hines A, Calvert D, Rutgersson A, Pettersson H, Bidlot J-R, Janssen PA, Polton JA (2012) A global perspective on Langmuir turbulence in the ocean surface boundary layer. *Geophys Res Lett* 39:L18605. doi:10.1029/2012GL052932
- Bertin X, Li K, Roland A, Bidlot JR (2015) The contribution of short-waves in storm surges: two case studies in the Bay of Biscay. *Cont Shelf Res* 96:1–15
- Bouillon S, Maqueda MA, Legat V, Fichefet T (2009) An elastic-viscous-plastic sea ice model formulated on Arakawa B and C grids. *Ocean Model* 27:174–184
- Breivik Ø, Mogensen K, Bidlot JR, Balmaseda MA, Janssen PAEM (2015) Surface wave effects in the NEMO ocean model: forced and coupled experiments. *J Geophys Res Oceans* 120:2973–2992
- Breivik Ø, Janssen PAEM, Bidlot J (2014) Approximate Stokes drift profiles in deep water. *J Phys Oceanogr* 44(9):2433–2445
- Carlsson B, Rutgersson A, Smedman AS (2009) Investigating the effect of a wave-dependent momentum flux in a process oriented ocean model. *Boreal Environ Res* 14(1):3–17
- Chang YC, Chen GY, Tseng RS, Centurioni LR, Chu PC (2012) Observed near-surface currents under high wind speeds. *J Geophys Res Oceans* 117:2156–2202
- Craig PD, Banner ML (1994) Modeling wave-enhanced turbulence in the ocean surface layer. *J Phys Oceanogr* 24(12):2546–2559
- Craik ADD, Leibovich S (1976) A rational model for Langmuir circulations. *J Fluid Mech* 73:401–426
- Dieterich C, Schimanke S, Wang S, Väli G, Liu Y, Hordoir R, Axell L, Hoeglund A, Meier HEM (2013) Evaluation of the SMHI coupled atmosphere-ice-ocean model RCA4-NEMO Rep. *Oceanogr* 4, 80 pp
- Dietrich JC, Zijlema M, Westerink JJ, Holthuijsen LH, Dawson C, Luettich RA, Jensen RE, Smith JM, Stelling GS, Stone GW (2011) Modeling hurricane waves and storm surge using integrally-coupled, scalable computations. *Coast Eng* 58(1):45–65
- Donlon CJ, Martin M, Stark JD, Roberts-Jones J, Fiedler E, Wimmer W (2011) The Operational Sea Surface Temperature and Sea Ice analysis (OSTIA) system. *Remote Sens Environ* 116:140–158
- Drennan WM, Donelan MA, Terray EA, Katsaros KB (1996) Oceanic turbulence dissipation measurements in SWADE. *J Phys Oceanogr* 26(5):808–815
- ECMWF (2015) CY41R1 Official IFS Documentation. <https://software.ecmwf.int/wiki/display/IFS/CY41R1+Official+IFS+Documentation>

- Gemmrich J (2010) Strong turbulence in the wave crest region. *J Phys Oceanogr* 40(3):583–595
- Gemmrich JR, Farmer DM (2004) Near-surface turbulence in the presence of breaking waves. *J Phys Oceanogr* 34(5):1067–1086
- Gemmrich JR, Mudge TD, Polonichko VD (1994) On the energy input from wind to surface waves. *J Phys Oceanogr* 24(11):2413–2417
- Grashorn S, Lettmann KA, Wolff JO, Badewien TH, Stanev EV (2015) East Frisian Wadden Sea hydrodynamics and wave effects in an unstructured-grid model. *Ocean Dyn* 65(3):419–434
- Hasselmann K (1970) Wave-driven inertial oscillations. *Geophys Fluid Dyn* 1(3–4):463–502
- Hordoir R, An BW, Haapala J, Dieterich C, Schimanke S, Hoeglund A, Meier HEM (2013) A 3D ocean modelling configuration for Baltic & North Sea exchange analysis. *Rep Oceanogr* 48:72
- Hu H, Wang J (2010) Modeling effects of tidal and wave mixing on circulation and thermohaline structures in the Bering Sea: Process studies. *J Geophys Res Oceans* 115(1), art. no. C01006
- Janssen PAEM (2012) Ocean wave effects on the daily cycle in SST. *J Geophys Res* 117:C00J32
- Janssen PAEM (1989) Wave-induced stress and the drag of air flow over sea waves. *J Phys Oceanogr* 19:745–754
- Janssen F, Schrum C, Backhaus JO (1999) A climatological data set of temperature and salinity for the Baltic Sea and the North Sea. *Deutsche Hydrographische Zeitschrift* 51(9 Supplement):5–245
- Kantha L, Lass HU, Prandke H (2010) A note on Stokes production of turbulence kinetic energy in the oceanic mixed layer: Observations in the Baltic Sea. *Ocean Dyn* 60(1):171–180
- Komen GJ, Cavaleri L, Donelan M, Hasselmann K, Hasselmann S, Janssen PAEM (1994) Dynamics and modelling of ocean waves. Cambridge Univ. Press, New York
- Lin X, Xie SP, Chen X, Xu L (2006) A well-mixed warm water column in the central Bohai Sea in summer: effects of tidal and surface wave mixing. *J Geophys Res-Oceans* 111(11), art. no. C11017
- Leppäranta M, Myrberg K (2009) Physical oceanography of the Baltic Sea. Springer, Berlin Heidelberg
- Longuet-Higgins MS, Stewart RW (1962) Radiation stress and mass transport in gravity waves, with application to ‘surf beats’. *J Fluid Mech* 13:481–504
- Madec G (2008) NEMO ocean engine. Note du Pole de modelisation. Institut Pierre-Simon Laplace (IPSL), France, No 27, ISSN No 1288–1619, 217 pp
- Masterbroek C, Burgers G, Janssen PAEM (1993) The dynamical coupling of a wave model and a storm surge model through the atmospheric boundary layer. *J Phys Oceanogr* 23:1856–1866
- Mellor G, Blumberg A (2004) Wave breaking and ocean surface layer thermal response. *J Phys Oceanogr* 34:693–698
- Pham TV, Brauch J, Dieterich C, Fruhe B, Ahrens B (2014) New coupled atmosphere–ocean–ice system COSMO-CLM/NEMO: assessing air temperature sensitivity over the North and Baltic Seas. *Oceanologia* 56(2):167–189
- Pleskachevsky A, Dobrynin M, Babanin AV, Günther H, Stanev E (2011) Turbulent mixing due to surface waves indicated by remote sensing of suspended particulate matter and its implementation into coupled modeling of waves, turbulence, and circulation. *J Phys Oceanogr* 41(4):708–724
- Pleskachevsky A, Eppel DP, Kapitza H (2009) Interaction of waves, currents and tides, and wave-energy impact on the beach area of Sylt Island. *Ocean Dyn* 59(3):451–461
- Polton JA, Lewis DM, Belcher SE (2005) The role of wave-induced Coriolis–Stokes forcing on the wind-driven mixed layer. *J Phys Oceanogr* 35:444–457
- Reistad M, Breivik O, Haakenstad H, Aarnes OJ, Furevik BR, Bidlot JR (2011). A high-resolution hindcast of wind and waves for the North Sea, the Norwegian Sea, and the Barents Sea. *J Geophys Res Oceans* 116, doi:10/fmnr2m
- Song Z, Qiao F, Song, Y (2012) Response of the equatorial basin-wide SST to non-breaking surface wave-induced mixing in a climate model: an amendment to tropical bias. *J Geophys Res Oceans* 117(7), art. no. C00J26
- Soomere T, Behrens A, Tuomi L, Nielsen JW (2008) Wave conditions in the Baltic Proper and in the Gulf of Finland during windstorm Gudrun. *Nat Hazard Earth Sys* 8(1):37–46
- Soomere T (2005) Wind wave statistics in Tallinn Bay. *Boreal Environ Res* 10:103–118
- Soomere T (2003) Anisotropy of wind and wave regimes in the Baltic proper. *J Sea Res* 49(4):305–316
- Qiao F, Yuan Y, Ezer T, Xia C, Yang Y, Lü X, Song Z (2010) A three-dimensional surface wave-ocean circulation coupled model and its initial testing. *Ocean Dyn* 60(5):1339–1355
- Qiao F, Yuan Y, Yang Y, Zheng Q, Xia C, Ma J (2004) Wave-induced mixing in the upper ocean: distribution and application to a global ocean circulation model. *Geophys Res Lett* 31(11):L11303 1–4
- Raudsepp U, Laanemets J, Haran G, Alari V, Pavelson J, Kõuts T (2011) Flow, waves and water exchange in the Suur strait, Gulf of Riga, in 2008. *Oceanologia* 53(1):35–56
- Schneggenburger C, Günther H, Rosenthal W (2000) Spectral wave modelling with non-linear dissipation: validation and applications in a coastal tidal environment. *Coast Eng* 41(1–3):201–235
- Stacey MW (1999) Simulations of the wind-forced near-surface circulation in Knight inlet: a parameterization of the roughness length. *J Phys Oceanogr* 29:1363–1367
- Stokes GG (1847) On the theory of oscillatory waves. *Trans Cambridge Philos Soc* 8:441–455
- Zambon JB, He R, Warner JC (2014) Investigation of hurricane Ivan using the coupled ocean–atmosphere–wave–sediment transport (COAWST) model. *Ocean Dyn* 64(11):1535–1554
- The WAMDI Group (1988) The WAM model—a third generation ocean wave prediction model. *J Phys Oceanogr* 18:1775–1810
- Terray EA, Donelan MA, Agrawal YC, Drennan WM, Kahma KK, Williams AJ, Hwang PA, Kitaigorodskii SA (1996) Estimates of kinetic energy dissipation under breaking waves. *J Phys Oceanogr* 26(5):792–807
- Tuomi L, Pettersson H, Fortelius C, Tikka K, Björkqvist JV, Kahma KK (2014) Wave modelling in archipelagos. *Coast Eng* 83:205–220
- Tuomi L, Myrberg K, Lehmann A (2012a) The performance of the parameterisations of vertical turbulence in the 3D modelling of hydrodynamics in the Baltic Sea. *Cont Shelf Res* 50–51:64–79
- Tuomi L, Kahma KK, Fortelius C (2012b) Modelling fetch-limited wave growth from an irregular shoreline. *J Mar Syst* 105–108:96–105
- Tuomi L, Kahma KK, Pettersson H (2011) Wave hindcast statistics in the seasonally ice-covered Baltic Sea. *Boreal Environ Res* 16(6):451–472
- Umlauf L, Burchard H (2003) A generic length-scale equation for geophysical turbulence models. *J Mar Res* 61(2):235–265
- Väli G, Meier HEM, Elken J (2013) Simulated halocline variability in the Baltic Sea and its impact on hypoxia during 1961–2007. *J Geophys Res Oceans* 118(12):6982–7000
- Warner JC, Armstrong B, He R, Zambon JB (2010) Development of a coupled ocean–atmosphere–wave–sediment transport (COAWST) modeling system. *Ocean Model* 35(3):230–244
- Whitham GB (1974) Linear and nonlinear waves. John Wiley & Sons, New York